Atmospheric
Chemistry
and Physics

Supplement of

Possible heterogeneous chemistry of hydroxymethanesulfonate (HMS) in northern China winter haze

Shaojie Song et al.

Correspondence to: Shaojie Song (songs@seas.harvard.edu), Yele Sun (sunyele@mail.iap.ac.cn), and Michael B. McElroy (mbm@seas.harvard.edu)

Supplement for acp-2018-1015

Shaojie Song et al. 2019

Supplementary Texts 1–4

Supplementary Figures 1–12

5   Supplementary Tables 1–3

Supplementary Texts

Text S1. Uncertainty quantification of HR-AMS measurements

The HR-AMS measurement uncertainties were estimated following Bahreini et al.[1]. The relative uncertainty $\left(\frac{\Delta_X}{X}\right)$ of mass concentration of the chemical species X (i.e., ammonium, sulfate, nitrate, chloride, organics, and black carbon) was quantified as

$$\frac{\Delta_X}{X} = \sqrt{\left(\frac{\Delta_{IE_{NO_3}}}{IE_{NO_3}}\right)^2 + \left(\frac{\Delta_{RIE_X}}{RIE_X}\right)^2 + \left(\frac{\Delta_{CE}}{CE}\right)^2 + \left(\frac{\Delta_Q}{Q}\right)^2 + \left(\frac{\Delta_{TE}}{TE}\right)^2} \tag{S1}$$

where $\frac{\Delta_{IE_{NO_3}}}{IE_{NO_3}}$, $\frac{\Delta_{CE}}{CE}$, $\frac{\Delta_Q}{Q}$, and $\frac{\Delta_{TE}}{TE}$ represent the relative uncertainties in the nitrate ionization efficiency (IE_{NO_3}), collection efficiency (CE), flow rate (Q), and transmission efficiency (TE), and were estimated to be 10%, 30%, <0.5%, and 10%, respectively. $\frac{\Delta_{RIE_X}}{RIE_X}$ represents the uncertainty in the ionization efficiency of the species X relative to nitrate (RIE_X), and depends on the species X (10% for ammonium, 15% for sulfate, and 20% for organics)[1]. Using the above equation, we estimated that the overall relative uncertainties of HR-AMS measurements were 33% (nitrate), 35% (ammonium), 36% (sulfate), and 39% (organics). The uncertainties for chloride were assumed to be 40%.

In order to quantify the uncertainty of sulfate-equivalent organosulfur concentration (C_{OS}), we rewrote Eq. (1) in the main text as

$$C_{OS} = \frac{M_{SO_4^{2-}}}{M_{SO^+}}\left(1 + \frac{M_{SO^+}}{M_{SO_2^+}}\frac{SO_{2,OS}^+}{SO_{OS}^+}\right) \times SO_{OS}^+ \tag{S2}$$

$$SO_{OS}^+ = \left(1 - \left(\frac{R_{cd,SO^+/SO_3^+}}{R_{obs,SO^+/SO_3^+}} + \frac{R_{cd,SO^+/HSO_3^+}}{R_{obs,SO^+/HSO_3^+}} + \frac{R_{cd,SO^+/H_2SO_4^+}}{R_{obs,SO^+/H_2SO_4^+}}\right)/3\right) \times SO_{obs}^+ \tag{S3}$$

$$SO_{2,OS}^+ = \left(1 - \left(\frac{R_{cd,SO_2^+/SO_3^+}}{R_{obs,SO_2^+/SO_3^+}} + \frac{R_{cd,SO_2^+/HSO_3^+}}{R_{obs,SO_2^+/HSO_3^+}} + \frac{R_{cd,SO_2^+/H_2SO_4^+}}{R_{obs,SO_2^+/H_2SO_4^+}}\right)/3\right) \times SO_{2,obs}^+ \tag{S4}$$

where SO_{OS}^+ and $SO_{2,OS}^+$ are the concentrations of the SO^+ and SO_2^+ ions attributable to OS, respectively. The observed ion ratios are defined as $R_{obs,SO^+/SO_3^+} = \frac{SO_{obs}^+}{SO_{3,obs}^+}$, $R_{obs,SO^+/HSO_3^+} = \frac{SO_{obs}^+}{HSO_{3,obs}^+}$, $R_{obs,SO^+/H_2SO_4^+} = \frac{SO_{obs}^+}{H_2SO_{4,obs}^+}$, $R_{obs,SO_2^+/SO_3^+} = \frac{SO_{2,obs}^+}{SO_{3,obs}^+}$, $R_{obs,SO_2^+/HSO_3^+} = \frac{SO_{2,obs}^+}{HSO_{3,obs}^+}$, and $R_{obs,SO_2^+/H_2SO_4^+} = \frac{SO_{2,obs}^+}{H_2SO_{4,obs}^+}$. $R_{cd,SO^+/SO_3^+}$, $R_{cd,SO^+/HSO_3^+}$, $R_{cd,SO^+/H_2SO_4^+}$, $R_{cd,SO_2^+/SO_3^+}$, $R_{cd,SO_2^+/HSO_3^+}$, and $R_{cd,SO_2^+/H_2SO_4^+}$ represent the average ratios of the two corresponding ions in the clean and dry periods. We further defined A and B and rewrote Eq. (S2)

$$A = 1 - \left(\frac{R_{cd,SO^+/SO_3^+}}{R_{obs,SO^+/SO_3^+}} + \frac{R_{cd,SO^+/HSO_3^+}}{R_{obs,SO^+/HSO_3^+}} + \frac{R_{cd,SO^+/H_2SO_4^+}}{R_{obs,SO^+/H_2SO_4^+}}\right)/3 \tag{S5}$$

$$B = 1 - \left(\frac{R_{cd,SO_2^+/SO_3^+}}{R_{obs,SO_2^+/SO_3^+}} + \frac{R_{cd,SO_2^+/HSO_3^+}}{R_{obs,SO_2^+/HSO_3^+}} + \frac{R_{cd,SO_2^+/H_2SO_4^+}}{R_{obs,SO_2^+/H_2SO_4^+}}\right)/3 \tag{S6}$$

$$C_{OS} = \frac{M_{SO_4^{2-}}}{M_{SO^+}}\left(1 + \frac{M_{SO^+}}{M_{SO_2^+}}\frac{B}{A}R_{obs,SO_2^+/SO^+}\right) \times SO_{obs}^+A \tag{S7}$$

where $R_{obs,SO_2^+/SO^+} = \frac{SO_{2,obs}^+}{SO_{obs}^+}$. The uncertainty of C_{OS} was calculated by propagating the uncertainties of each term in

Eqs. (S5–S7). The uncertainties of $R_{cd,SO^+/SO_3^+}$, $R_{cd,SO^+/HSO_3^+}$, $R_{cd,SO^+/H_2SO_4^+}$, $R_{cd,SO_2^+/SO_3^+}$, $R_{cd,SO_2^+/HSO_3^+}$, and $R_{cd,SO_2^+/H_2SO_4^+}$

were estimated by the standard deviations of the corresponding ion ratios observed during the clean and dry periods.

The uncertainties of $R_{obs,SO_2^+/SO^+}$, $R_{obs,SO^+/SO_3^+}$, $R_{obs,SO^+/HSO_3^+}$, $R_{obs,SO^+/H_2SO_4^+}$, $R_{obs,SO_2^+/SO_3^+}$, $R_{obs,SO_2^+/HSO_3^+}$, and

$R_{obs,SO_2^+/H_2SO_4^+}$ were obtained by the standard deviations of the 5-minute samples in each hour. The relative uncertainty

of SO_{obs}^+ was estimated by Eq. (S1) assuming the same RIE as sulfate.

Text S2. Mass transfer of heterogeneous HMS production

In order to examine whether the production of HMS was limited by the kinetics of mass transport, we estimated the

characteristic time scales (τ) for the HMS chemical reaction, the mass transfer steps (including gas-phase diffusion,

interfacial transport, hydrolysis/ionization, and aqueous-phase diffusion), and formaldehyde hydration. The average

values during winter haze episodes ($PM_1 > 100$ μg m^{-3}) were used in our calculation: $[SO_{2(g)}] = 14$ ppb, $[HCHO_{(g)}]$

$= 10$ ppb, $T = 278$ K, $PM_1 = 160$ μg m^{-3}, and AWC $= 100$ μg m^{-3}. The characteristic times for the chemical loss of

SO_2 and HCHO, τ_{r,SO_2} and $\tau_{r,HCHO}$, were estimated by

$$\tau_{r,SO_2} = \left\{(k_1\alpha_1 + k_2\alpha_2)[HCHO_{(aq)}]\right\}^{-1} \text{ and } \tau_{r,HCHO} = \left\{(k_1\alpha_1 + k_2\alpha_2)[SO_{2(aq)}]\right\}^{-1} \tag{S8}$$

For a chemical species A (SO_2 or HCHO), the characteristic time, $\tau_{dg\&phase}$, that includes the gas-phase diffusion and

the establishment of phase equilibrium at the interface of aqueous aerosol particles was expressed as[2]

$$\tau_{dg\&phase} = \frac{H_A^*RT\rho_p R_p^2 \cdot AWC}{3m_pD_{g,A}f(Kn,\alpha)} \tag{S9}$$

where H_A^* is the effective Henry's law constant of A (M atm^{-1}), R is the gas constant, T is the temperature (K), ρ_p is

the aerosol droplet density and estimated to be 1.3×10^3 kg m^{-3}, R_p is the average aerosol droplet radius assumed as

0.15 μm following ref.[3], m_p is the aerosol droplet mass concentration (~260 μg m^{-3}), $D_{g,A}$ is the gas-phase diffusion

coefficient of A in the air (m^2 s^{-1})[4,5], and $f(Kn,\alpha)$ is the correction factor to mass transfer flux owing to non-continuum

effects and imperfect accommodation[6]

$$f(Kn,\alpha) = 0.75\alpha\,(1 + Kn)\left(Kn^2 + Kn + 0.283Kn\alpha + 0.75\alpha\right)^{-1} \tag{S10}$$

where α is the mass accommodation coefficient of A on aqueous surfaces, and the Knudsen number is given by

$$Kn = \frac{3D_{g,A}}{R_p}\sqrt{\frac{\pi M_A}{8RT}} \tag{S11}$$

3

where M_A is the molar mass of A. The characteristic time for aqueous-phase diffusion, τ_{da}, was quantified by[2]

$$\tau_{da} = \frac{R_p^2}{\pi^2 D_{aq}} \tag{S12}$$

where D_{aq} is the aqueous-phase diffusion coefficient (a typical value: 10^{-9} m^2 s^{-1}). The characteristic times, τ_{i1} and τ_{i2}, are respectively associated with the hydrolysis/ionization equilibria of $SO_{2(aq)}$ ($SO_2 \cdot H_2O \leftrightarrow HSO_3^- + H^+$ and HSO_3^- $\leftrightarrow SO_3^{2-} + H^+$) and were estimated following Schwartz and Freiberg[7]

$$\tau_{i1} = \left\{ 3 \times 10^6 \text{ s}^{-1} + 2 \times 10^8 \text{ M}^{-1} \text{ s}^{-1} \times \left([H^+] + [HSO_3^-] \right) \right\}^{-1} \tag{S13}$$

$$\tau_{i2} = \left\{ 2 \times 10^3 \text{ s}^{-1} + 3 \times 10^{10} \text{ M}^{-1} \text{ s}^{-1} \times \left([H^+] + [SO_3^{2-}] \right) \right\}^{-1} \tag{S14}$$

The characteristic time for the hydration of HCHO, τ_{hyd}, was estimated using the hydration rate constant k_{hyd} (s^{-1})

$$\tau_{hyd} = k_{hyd}^{-1} \tag{S15}$$

As shown in Fig. S11, the time scales of the mass transfer processes ($\tau_{dg\&phase}$, τ_{da}, τ_{i1}, and τ_{i2}) were much smaller than those of chemical reaction (τ_r) and HCHO hydration (τ_{hyd}), suggesting that the mass transfer and HCHO hydration were not rate-limiting for HMS production in aerosol water.

Text S3. Production of other hydroxyalkylsulfonate species

It is known that many aldehydes can undergo nucleophilic addition reactions with SO_2 to form HAS in the aqueous phase through a similar chemical mechanism with HCHO[8]. The importance of different aldehydes in the production of HAS depends on several factors including their gas-phase levels, water solubility, and kinetic and thermodynamic data. Most aldehydes already identified in the polluted atmosphere, such as acetaldehyde, propanal, butanal, pentanal, hexanal, and benzaldehyde, contribute insignificantly to HAS owing to low reaction rates. Four aldehydes, including glyoxal, methylglyoxal, glycolaldehyde, and glyoxylic acid, have similar or larger reaction rate constants compared to formaldehyde[8], and are thus worthy of further discussion. The properties of these aldehydes and their corresponding HAS species are given in Table S3.

In order to evaluate the relative importance of these aldehydes, we calculated their HAS formation rates, equilibrium concentrations, and characteristic times to reach equilibrium, using the average observational and model data ($[SO_{2(g)}]$ = 14 ppb, $[HCHO_{(g)}]$ = 10 ppb, T = 278 K, and AWC = 100 μg m^{-3}) obtained during Beijing winter haze periods (PM$_1$ > 100 μg m^{-3}). In the calculations, we assumed that these aldehydes had the same gaseous concentrations: $[RCHO_{(g)}]$ = 10 ppb. Although these aldehydes (methylglyoxal, glyoxal, glycolaldehyde, and glyoxylic acid) exhibited faster formation rates compared with formaldehyde, their equilibrium concentrations were much smaller, and it usually took less than a few hours for them to reach equilibrium (Fig. S12). Also considering that their gas-phase concentrations are typically one to two orders of magnitude lower than that of formaldehyde in the polluted environment[9-11], we suggest that these aldehydes are much less important in the formation of HAS species compared to formaldehyde. In addition, the characteristic times to reach equilibrium for formaldehyde were found about 2–40

days for pH range of winter haze aerosols (4.1–5.5), larger than typical time scales of haze accumulation (less than a day)[12], and therefore, the HMS in aerosols were usually not in equilibrium with HCHO and SO_2 in the gas phase.

Text S4. Influence of ionic strength on HMS production

5　　The relationship between the reaction rate constants (k) of HMS formation and the solution ionic strengths (I) has not been studied experimentally, and can only be estimated theoretically. The rate-limiting step of HMS production is the nucleophilic addition of an anion (HSO_3^- or SO_3^{2-}) to a neutral molecule (HCHO). For this type of reaction, the k–I relationship can be expressed by the kinetic salting coefficient b[13]

$$\log(k/k^{I=0}) = bI \tag{S16}$$

10　　where $k^{I=0}$ represents the reaction rate constant in an ideal-dilute solution ($I = 0$ M). It is known that b is related to the water solubility of the neutral species[13] (i.e., HCHO), and according to ref.[14], the value of b is expected to be positive. Thus, the actual reaction rate constants (k) in aerosol water droplets (with an average I of ~11 M during haze periods) should be enhanced compared with dilute electrolyte solutions. It is noted that the kinetic salt effects may also depend on the nature of electrolytes present in the solution.
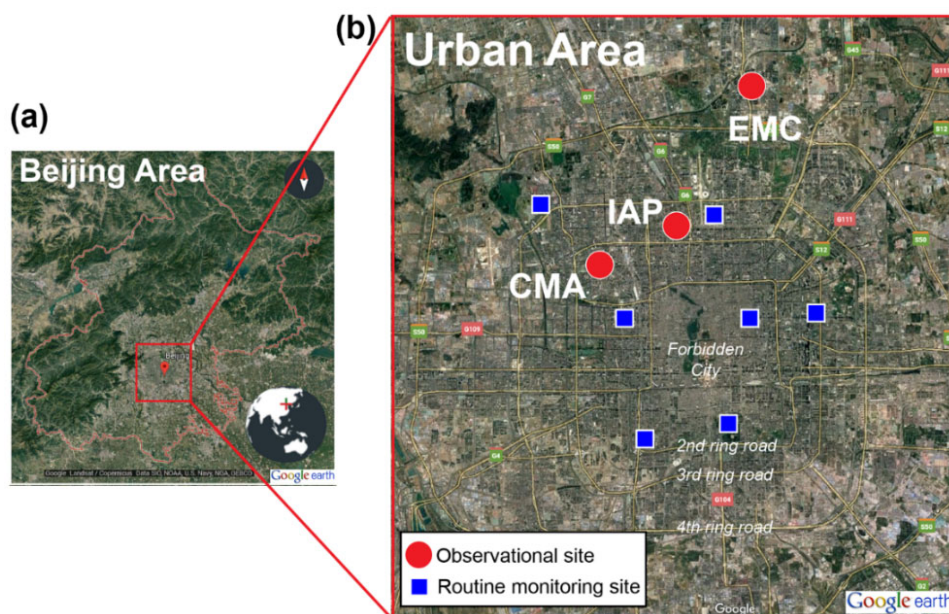
Supplementary Figures

Figure S1. Location of observational sites in urban Beijing. (a) Map of Beijing area. (b) Sites in the urban area of Beijing city. The CMA, IAP, and EMC sites were located in the Chinese Academy of Meteorological Sciences (39.95°N, 116.33°E), the Institute of Atmospheric Physics of the Chinese Academy of Sciences (39.98°N, 116.38°E), and the China National Environmental Monitoring Centre (40.04°N, 116.42°E), respectively. The levels of air pollutants at the IAP site compared well with results from the routine urban monitoring sites of Beijing municipal environmental monitoring center (*www.bjmemc.com.cn*, last access: 24 September 2018), suggesting the homogeneity of air pollution in urban Beijing and the representativeness of observational sites.
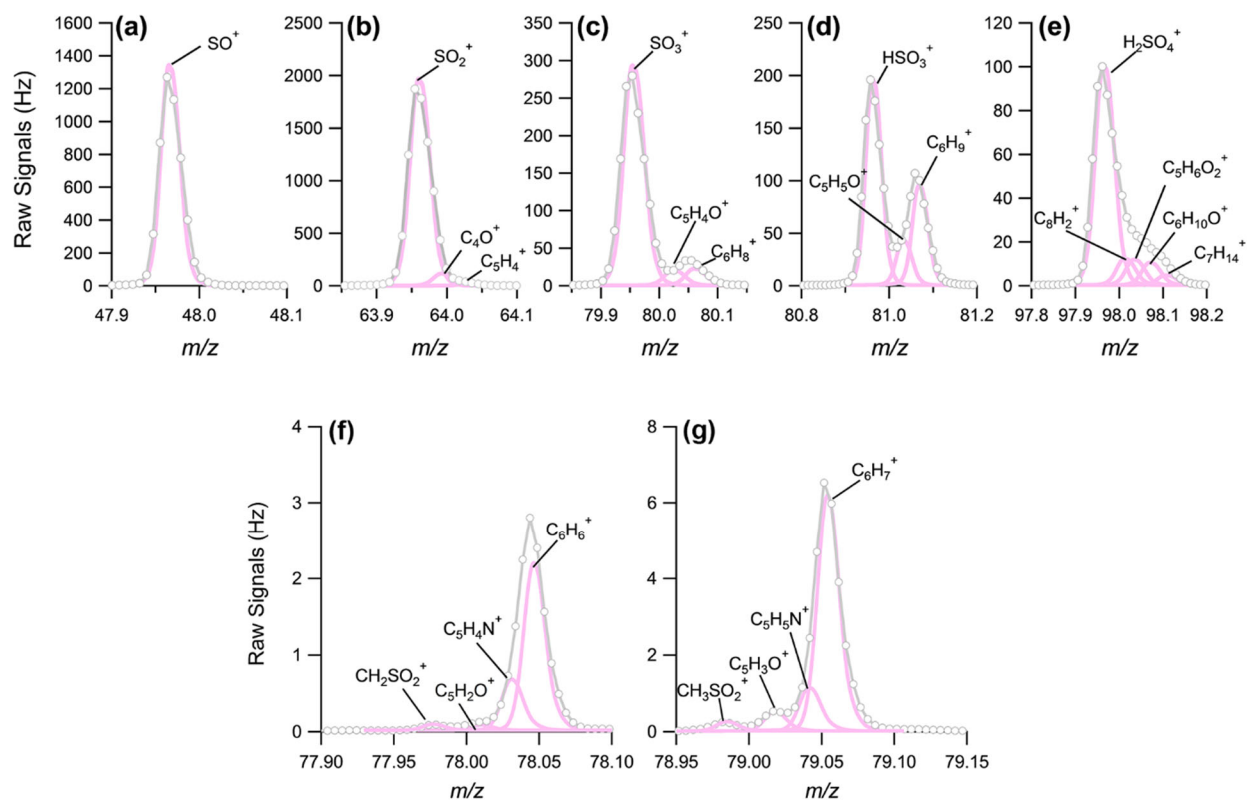
Figure S2. Examples of the raw signals and fitted peaks of inorganic and organic sulfur-containing fragment ions in the HR-AMS field measurements. (a) SO^+ (*m/z* 48), (b) SO_2^+ (*m/z* 64), (c) SO_3^+ (*m/z* 80), (d) HSO_3^+ (*m/z* 81), (e) $H_2SO_4^+$ (*m/z* 98), (f) $CH_2SO_2^+$ (*m/z* 78), and (g) $CH_3SO_2^+$ (*m/z* 79). (a–e) show the V-mode mass spectra data and (f–g) show the W-mode data.
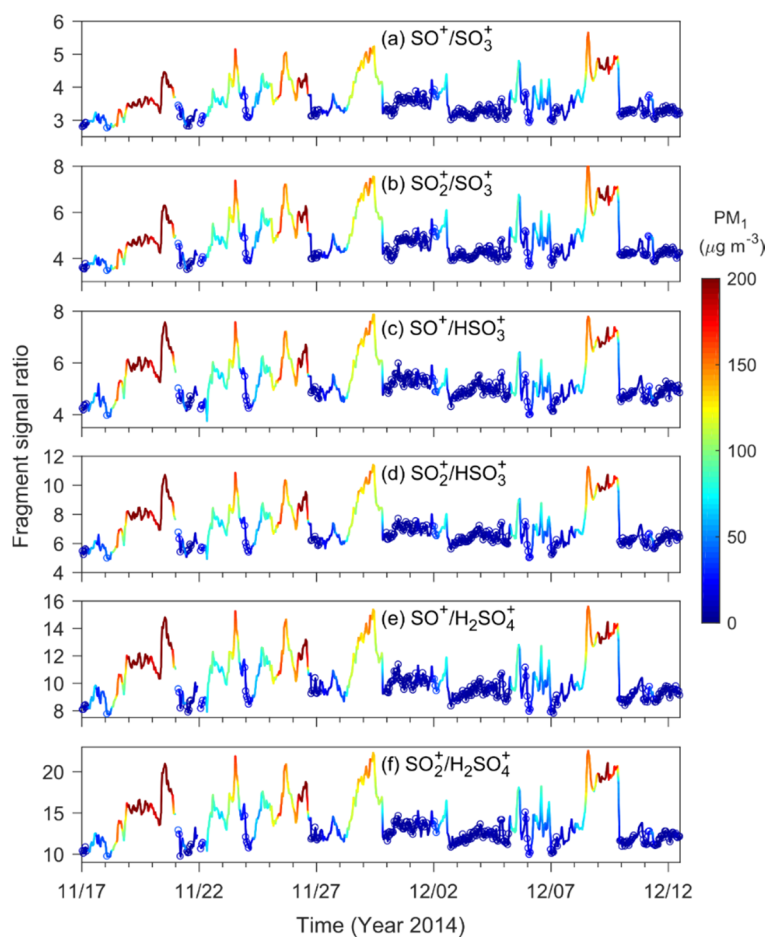
Figure S3. Time series of HR-AMS signal ratios of inorganic sulfur-containing fragment ions during winter 2014 in urban Beijing. (a) SO^+/SO_3^+, (b) SO_2^+/SO_3^+, (c) SO^+/HSO_3^+, (d) SO_2^+/HSO_3^+, (e) $SO^+/H_2SO_4^+$, and (f) $SO_2^+/H_2SO_4^+$. The circles indicate the observations under clean and dry conditions (filtered by $PM_1 < 50$ µg m^{-3}, RH < 30%, and $O_3 > 10$ ppb). The curves and circles are colored according to the observed PM_1 concentrations. The haze conditions are defined as $PM_1 > 100$ µg m^{-3}.

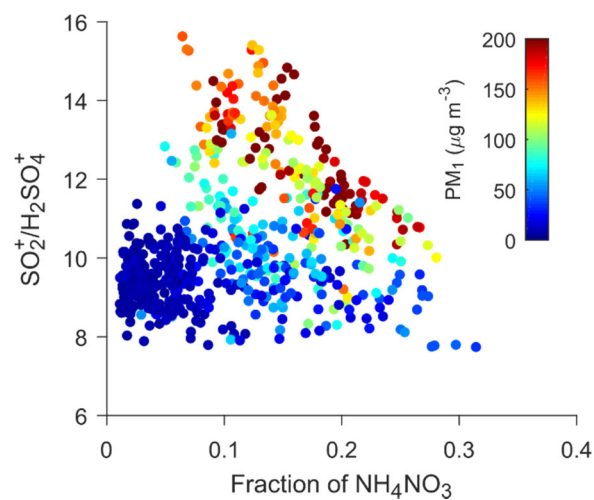**Figure S4.** Relationship between $SO_2^+/H_2SO_4^+$ and fraction of ammonium nitrate. The dots are colored according to PM_1 mass concentrations.
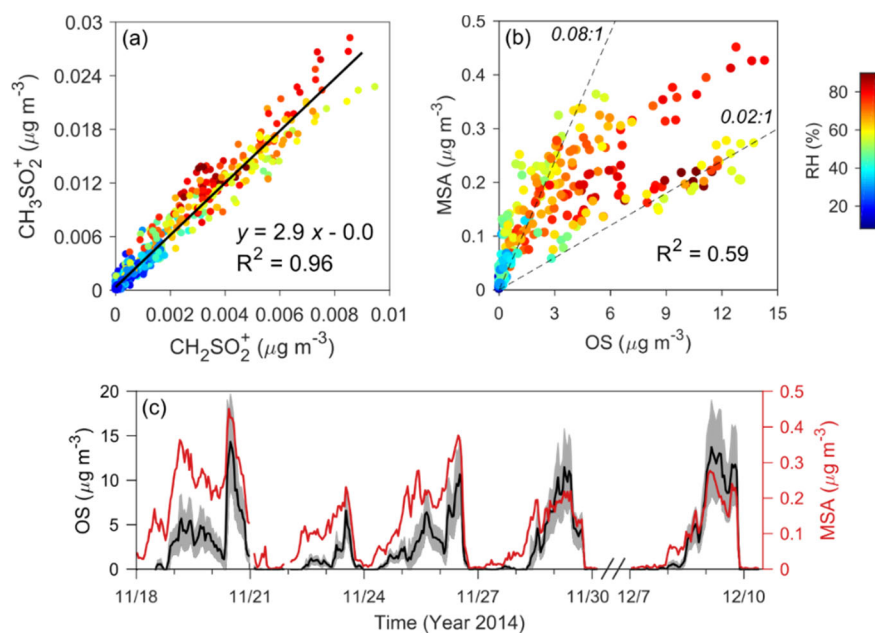

Figure S5. Methanesulfonate (or MSA) in Beijing winter aerosols estimated by HR-AMS. (a) Linear correlation of the observed hourly concentrations of fragment ions $CH_3SO_2^+$ and $CH_2SO_2^+$. (b) Scatter plot and (c) Time series of the identified sulfate-equivalent OS and methanesulfonate (or MSA) concentrations. The dots in (a–b) are colored according to RH. The shaded region in (c) indicates the 1-σ uncertainty range of OS.
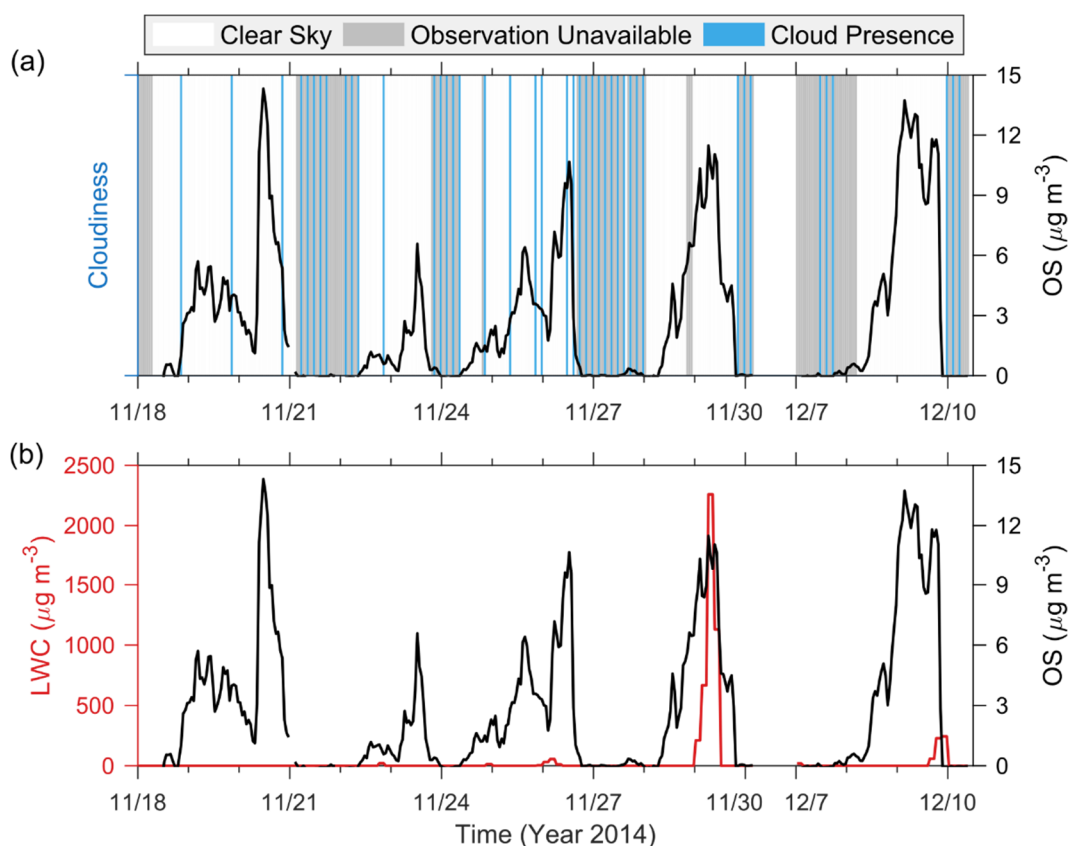
Figure S6. Relationship between the sulfate-equivalent OS concentrations and cloud/fog information in Beijing winter. (a) Time series of OS and cloud cover as observed at the Beijing Capital International Airport. Blue, white, and gray colors indicate cloud presence, clear sky, and observation unavailable, respectively. Cloud cover data were obtained from the NOAA's National Climatic Data Center (NCDC) Integrated Surface Database (ISD)[15]. (b) Time series of OS and cloud/fog liquid water content (LWC) during 2014 winter in Beijing. LWC was obtained from the MERRA-2 reanalysis meteorology (Modern-Era Retrospective analysis for Research and Applications, Version 2)[16]. The average LWC over the Beijing area and below 1 km (assumed as the upper limit of the planetary boundary layer height during Beijing winter haze periods[17-19]) is calculated and shown.
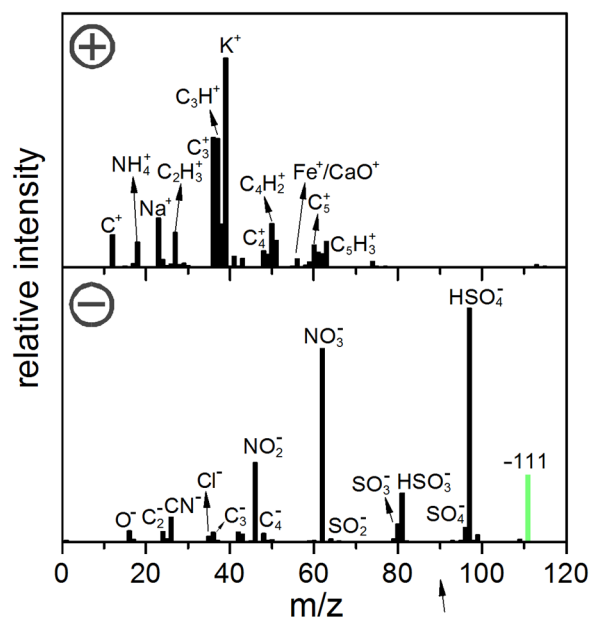
10

Figure S7. Average positive (+) and negative (−) ion mass spectra of HMS-containing individual particles from the SPAMS analysis. The m/z −111 peak was attributed to HMS. The m/z −81 HSO_3^-, m/z −80 SO_3^-, and m/z −64 SO_2^- peaks likely resulted from the fragmentation of HMS. The negative mass spectra also suggested the presence of nitrate (m/z −46 NO_2^- and m/z −62 NO_3^-), sulfate (m/z −96 SO_4^- and m/z −97 HSO_4^-), and carbonaceous species (e.g., m/z −16 O^-, m/z −24 C_2^-, and m/z −26 CN^-). The positive mass spectra featured m/z +18 NH_4^+, m/z +39 K^+, m/z +23 Na^+, and carbonaceous species (e.g., m/z +21 C^+ and m/z +27 $C_2H_3^+$). The response of different species varied in the single particle mass spectrometry owing to their difference in ionization energy and matrix effects. Some species such as Na^+ and K^+ were more sensitive in the mass spectra because their ionization energies are low[20].
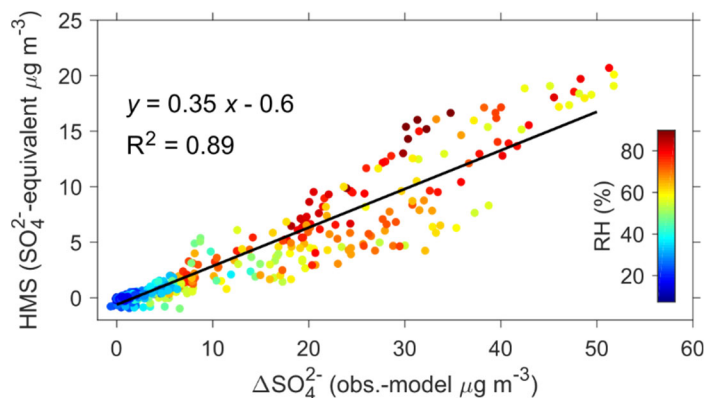

Figure S8. Contribution of HMS to the missing sulfate (ΔSO_4^{2-}) concentrations, if the identified OS resided only in the form of HMS. The HR-AMS mass spectra of standard HMS obtained from refs.[21,22] were used for estimation.
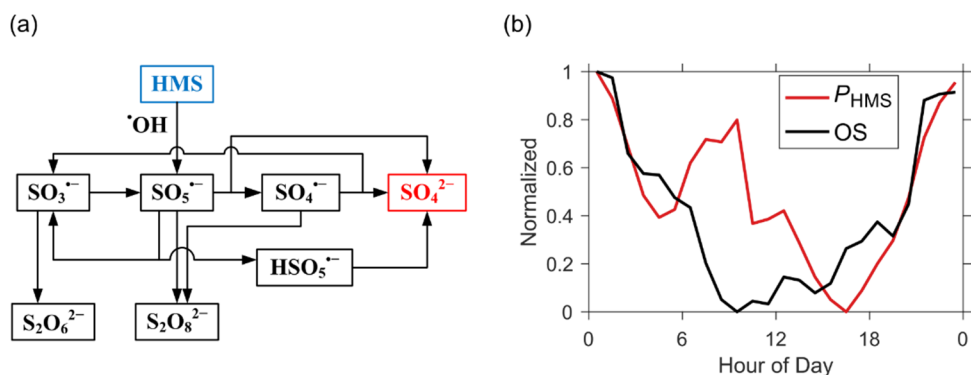
Figure S9. The possible role of HMS chemistry in the missing sulfate problem. (a) Schematic of reactions in the radical oxidation chain of HMS by the OH radical. (b) Average normalized diurnal profiles of HMS production rate (P_{HMS}) and OS concentrations.
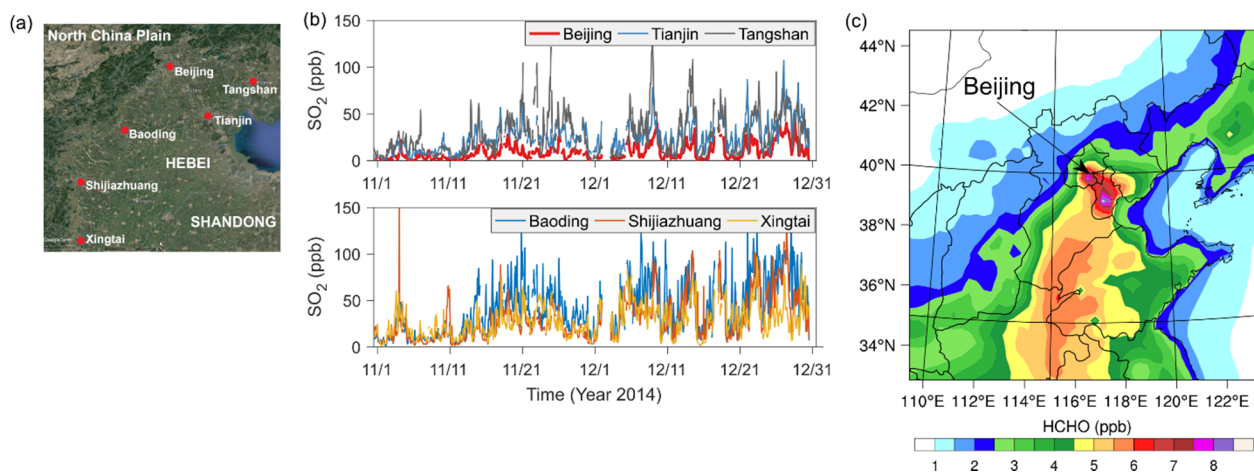
5

Figure S10. Regional pollution of SO_2 and HCHO across the NCP during winter 2014. (a) Topographic map around Beijing, and location of cities shown in (b). (b) SO_2 concentrations in Beijing and its southwest and southeast cities. (c) Distribution of HCHO from WRF-Chem model simulations.
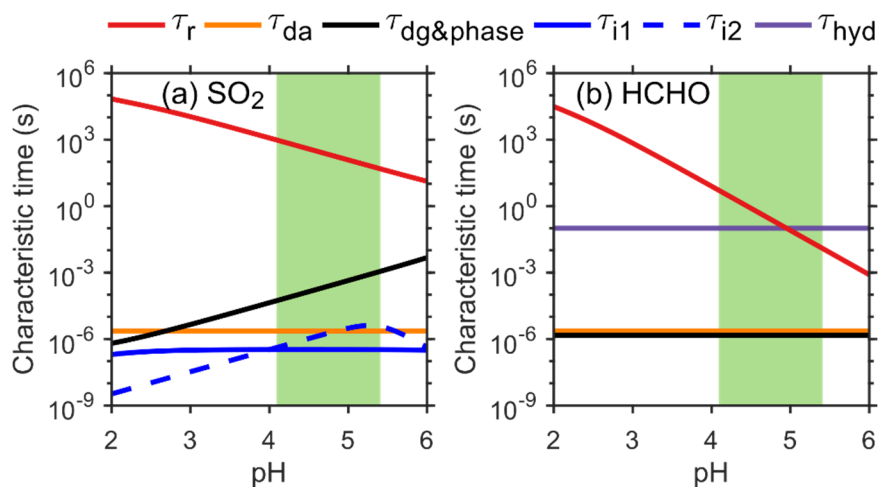
Figure S11. The characteristic times of mass transfer and chemical reaction for HMS production. (a) and (b) show the characteristic time scales (τ) of SO_2 and HCHO, respectively (defined in Text S2). The green shaded regions indicate the relevant aerosol water pH range of winter haze.

5
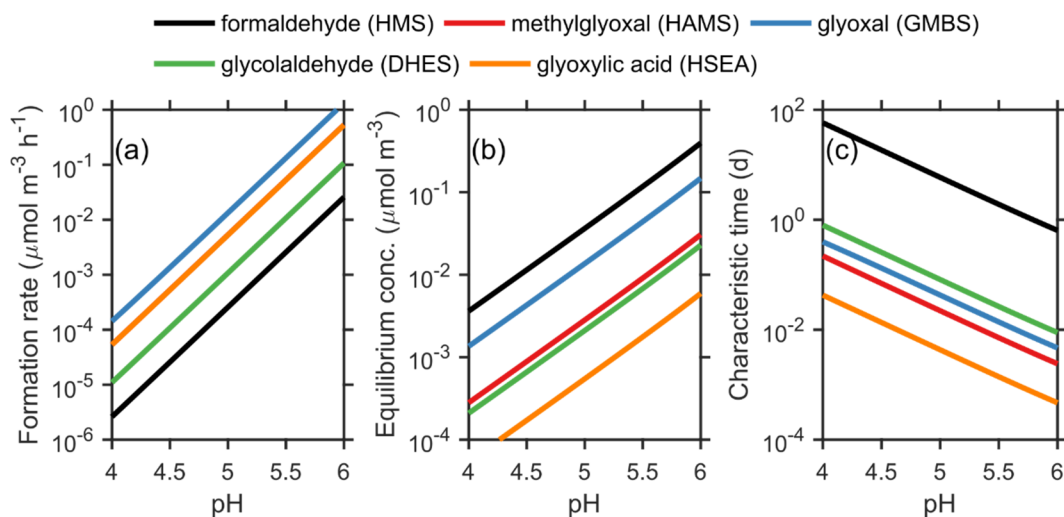
Figure S12. Comparison of the relative importance of several aldehydes in the formation of HAS. (a), (b), and (c) respectively show the calculated HAS formation rates, equilibrium concentrations, and characteristic times to reach equilibrium for five aldehydes (formaldehyde, methylglyoxal, glyoxal, glycolaldehyde, and glyoxylic acid), using the average measurement and model data obtained during Beijing winter haze periods (2014 winter).

13

Supplementary Tables

Table S1. Summary of experimental methods in the field measurements.

Species	Instrument	Site	Time resolution	Period (2014)
PM_1, ammonium, sulfate, nitrate, chloride, organics, and S-containing fragment ions	High-resolution time-of-flight aerosol mass spectrometer (HR-AMS; Aerodyne Research, Inc., USA)	IAP	5 min	11/17 to 12/12
$PM_{0.2-2}$, fragment ions at different m/z	Single particle aerosol mass spectrometer (SPAMS; Hexin Analytical Instrument Co., China)	EMC	10 min	12/4 to 12/12
$PM_{2.5}$, black carbon	Aethalometer Model AE33	IAP	1 min	11/17 to 12/12
Gas NH_3, HNO_3, and HCl	Gas and Aerosol Collector Ion Chromatography (GAC-IC)	IAP	30 min	11/17 to 12/12
Gas HCHO	AL4021 analyzer (Aero Laser GmbH, Germany)	CMA	2 min	12/1 to 12/15
Gas SO_2 and O_3	Model 43i and 49i analyzers (Thermo Fisher Scientific Inc., USA)	IAP	1 min	11/17 to 12/15
Temperature and relative humidity	Rotronic HC2-S3 probe	IAP	1 min	11/17 to 12/15

Table S2. Physical and chemical constants of SO_2.

Symbol	Value	Note	Source
α, dimensionless	0.11	Mass accommodation coefficient on aqueous surfaces	ref. [2]
H_{298}, M atm^{-1} ($-\Delta H/R$, K)	1.3 (3100)	$SO_{2(g)} + H_2O \leftrightarrow SO_2 \cdot H_2O$	ref. [23]
K_{s1}, M ($-\Delta H/R$, K)	1.3×10^{-2} (2000)	$SO_2 \cdot H_2O \overset{K_{s1}}{\leftrightarrow} HSO_3^- + H^+$	ref. [2]
K_{s2}, M ($-\Delta H/R$, K)	6.6×10^{-8} (1500)	$HSO_3^- \overset{K_{s2}}{\leftrightarrow} SO_3^{2-} + H^+$	ref. [2]

The dependence of H at a given temperature T is expressed below and similar expressions apply to K_{s1} and K_{s2}.
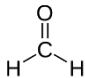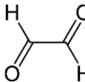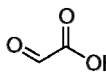
$$H(T) = H_{298} \exp\left[\frac{-\Delta H}{R}\left(\frac{1}{T} - \frac{1}{298}\right)\right]$$

The fractions of HSO_3^- and SO_3^{2-} in $SO_{2(aq)}$, α_1 and α_2, respectively, are determined by

$$\alpha_1 = \frac{K_{s1}[H^+]}{[H^+]^2 + K_{s1}[H^+] + K_{s1}K_{s2}} \text{ and } \alpha_2 = \frac{K_{s1}K_{s2}}{[H^+]^2 + K_{s1}[H^+] + K_{s1}K_{s2}}$$

where K_{s1} and K_{s2} are the corresponding acid dissociation constants (M), and $[H^+]$ refers to the hydrogen ion activity (M).

Table S3. Physical and chemical properties of several aldehydes and their corresponding hydroxyalkylsulfonates.

Aldehydes (RCHO)					
Aldehyde	formaldehyde	methylglyoxal	glyoxal[a]	glycolaldehyde	glyoxylic acid[b]
Other name(s)	methanal	pyruvaldehyde; propanonal	ethanedial	hydroxyacetaldehyde; 2-hydroxyethanal	oxoacetic acid; oxoethanoic acid
Formula	HCHO	CH_3COCHO	CHOCHO	$HOCH_2CHO$	HO_2CCHO
Structure					
H_{298}, **M atm^{-1} ($-\Delta H/R$, K)**	2.5^c (3300^d)	1.4^c (N.A.)	1.9^e (N.A.)	4.1×10^{3c} (N.A.)	29^e (N.A.)
H^{*}_{298}, **M atm^{-1} ($-\Delta H/R$, K)**	3.2×10^{3f} (7100^f)	3.7×10^{3c} (7500^c)	4.1×10^{5f} (7500^f)	4.1×10^{4c} (4600^c)	1.1×10^{4f} (4800^f)
k_{hyd} **at 298 K, s^{-1}**	$10^{g,h}$	20^g	10^i	N.A.	10^g
α, **dimensionless**	0.02^j	$\geqslant 1 \times 10^{-4k}$	0.02^i	N.A.	N.A.

Hydroxyalkylsulfonates (HAS)					
Hydroxyalkylsulfonate	hydroxymethanesulfonate	hydroxyacetylmethanesulfonate	1-hydroxy-2,2-diol-1-ethanesulfonate (or glyoxal monobisulfite)	1,2-dihydroxy-1-ethanesulfonate	2-hydroxy-2-sulfo-ethanoic acid
Abbreviation	HMS	HAMS	GMBS[a]	DHES	HSEA
Formula	$CH_2(OH)SO_3^-$	$CH_3COCH(OH)SO_3^-$	$CH(OH)_2CH(OH)SO_3^-$	$CH_2(OH)CH(OH)SO_3^-$	$HO_2CCH(OH)SO_3^-$
k_1, **M^{-1} s^{-1} ($-E/R$, K)**	7.9×10^2 (-4900^l)	3.5×10^3 (-3500^m)	3×10^4 (N.A.)^n	1.7 (-3600°)	4.4×10^2 (-2600^p)
k_2, **M^{-1} s^{-1} ($-E/R$, K)**	2.5×10^7 (-1800^l)	3.7×10^8 (-2200^m)	4×10^8 (N.A.)^n	5.0×10^4 (-2100°)	2.0×10^7 (N.A.)^p
K_{eq}, **M^{-1} ($-\Delta H/R$, K)**	$(5\text{–}9) \times 10^9$ (10000^q)	8×10^8 (6600^m)	6×10^9 (3500^n)	2×10^6 (N.A.)^g	7×10^7 (N.A.)^p

N.A. = not available. H, H^{*}, and K_{eq} have similar expressions of temperature dependence as those for SO_2. The temperature dependence of the reaction rate constants k (k_1 or k_2) is
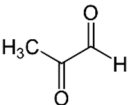
$$k(T) = k(298) \exp\left(\frac{-E}{R}\left(\frac{1}{T} - \frac{1}{298}\right)\right)$$

[a]The mechanism for glyoxal is more complicated than those for other aldehydes as glyoxal has two aldehyde groups. Both free CHOCHO and its monohydrated form CH(OH)$_2$CHO can react with SO$_{2(aq)}$ to form hydroxyalkylsulfonates: CHOCHO + HSO$_3^-$ ↔ CHOCH(OH)SO$_3^-$, CHOCHO + SO$_3^{2-}$ ↔ CHOCH(O$^-$)SO$_3^-$, CH(OH)$_2$CHO + HSO$_3^-$ ↔ CH(OH)$_2$CH(OH)SO$_3^-$, and CH(OH)$_2$CHO + SO$_3^{2-}$ ↔ CH(OH)$_2$CH(O$^-$)SO$_3^-$. The intrinsic rate constants for the above individual nucleophilic addition reactions were not determined, whereas the apparent rate constants for the total dissolved glyoxal (CHOCHO + CH(OH)$_2$CHO + (CH(OH)$_2$)$_2$) were obtained in laboratory experiments[24]. For the sake of simplicity, we assume that the nucleophilic addition of CH(OH)$_2$CHO is insignificant compared with CHOCHO, and, accordingly, the intrinsic rate constants for CHOCHO + HSO$_3^-$ ↔ CHOCH(OH)SO$_3^-$ and CHOCHO + SO$_3^{2-}$ ↔ CHOCH(O$^-$)SO$_3^-$ can be derived from the apparent rate constants and the equilibrium constants of glyoxal hydration[23-25]. It is important to note that this simplification may lead to an overestimation of the actual formation rates of GMBS, and therefore the listed values of k_1 and k_2 should be regarded as the upper limits. GMBS can further react with SO$_{2(aq)}$ to form GDBS (1,2-dihydroxy-1,2-ethanesulfonate or glyoxal dibisulfite, (CH(OH)SO$_3^-$)$_2$): GMBS + SO$_{2(aq)}$ ↔ GDBS. The formation of GDBS is not considered since the kinetic and thermodynamic data remain unclear.

[b]Glyoxylic acid may dissociate in aqueous solution, HO$_2$CCHO ↔ H$^+$ + $^-$O$_2$CCHO, with a pK_a of about 2[26]. Note that HO$_2$CCHO is the reactive carbonyl species and that $^-$O$_2$CCHO does not contribute significantly to the nucleophilic addition with SO$_{2(aq)}$.[8] HSEA may dissociate in aqueous solution, HO$_2$CCH(OH)SO$_3^-$ ↔ H$^+$ + $^-$O$_2$CCH(OH)SO$_3^-$, with a pK_a of about 3[26].

[c]From the compilation by ref. [27].

[d]Inferred from $-\Delta H/R$ = 7100 K for the effective Henry's law constant H^* and $-\Delta H/R$ = 3800 K for the hydration equilibrium constant HCHO + H$_2$O ↔ CH$_2$(OH)$_2$[23,28].

[e]Ref. [25].

[f]From the compilation by ref. [23].

[g]From the compilation by ref. [8].

[h]Ref. [28] derived an expression for the reaction rate constant of formaldehyde hydration: k_{hyd} = 2.0 × 10^5 × exp($-$2900/T) s^{-1}, which decreases with the ambient temperature.

[i]Ref. [29]. k_{hyd} data are for the first step hydration of glyoxal: CHOCHO + H$_2$O ↔ CH(OH)$_2$CHO.

[j]From the compilation by ref. [2].

[k]From the compilation by ref. [30].

[l]Ref. [31]. Experiments were conducted at I = 1.0 M, 0.7 ≤ pH ≤ 3.5.

[m]Ref. [32]. Experiments were conducted at I = 0.2 M, 0.7 ≤ pH ≤ 2.

[n]Ref. [24]. Experiments were conducted at I = 0.2 M, 0.7 ≤ pH ≤ 3.3.

[o]Ref. [33]. Experiments were conducted at I = 0.2 M, 0.7 ≤ pH ≤ 3.3.

[p]Ref. [26]. Experiments were conducted at I = 0.2 M, 0.7 ≤ pH ≤ 2.9.

[q]Derived from ref. [28,34-36]. K_{eq} remains unchanged over the pH range from 3 to 7 (when HSO$_3^-$ is the dominant SO$_{2(aq)}$ species).

Supplementary References

1. Bahreini, R. et al. Organic aerosol formation in urban and industrial plumes near Houston and Dallas, Texas. *J. Geophys. Res.-Atmos.* **114**, D00F16 (2009).

2. Seinfeld, J. H., Pandis, S. N. *Atmospheric chemistry and physics: from air pollution to climate change*, Third edn. John Wiley & Sons, Inc. (2016).

3. Cheng, Y. et al. Reactive nitrogen chemistry in aerosol water as a source of sulfate during haze events in China. *Sci. Adv.* **2**, e1601530 (2016).

4. Kimbell, J. S., Subramaniam, R. P., Gross, E. A., Schlosser, P. M., Morgan, K. T. Dosimetry modeling of inhaled formaldehyde: comparisons of local flux predictions in the rat, monkey, and human nasal passages. *Toxicol. Sci.* **64**, 100-110 (2001).

5. Tang, M. J., Cox, R. A., Kalberer, M. Compilation and evaluation of gas phase diffusion coefficients of reactive trace gases in the atmosphere: volume 1. Inorganic compounds. *Atmos. Chem. Phys.* **14**, 9233-9247 (2014).

6. Fuchs, N. A., Sutugin, A. G. High-dispersed aerosols. In: *Topics in Current Aerosol Research* (eds Brock J. R.). Pergamon (1971).

7. Schwartz, S. E., Freiberg, J. E. Mass-transport limitation to the rate of reaction of gases in liquid droplets: Application to oxidation of SO_2 in aqueous solutions. *Atmos. Environ.* **15**, 1129-1144 (1981).

8. Olson, T. M., Hoffmann, M. R. Hydroxyalkylsulfonate formation: Its role as a S(IV) reservoir in atmospheric water droplets. *Atmos. Environ.* **23**, 985-997 (1989).

9. Lui, K. H. et al. Spatial distributions of airborne di-carbonyls in urban and rural areas in China. *Atmos. Res.* **186**, 1-8 (2017).

10. Rao, Z., Chen, Z., Liang, H., Huang, L., Huang, D. Carbonyl compounds over urban Beijing: concentrations on haze and non-haze days and effects on radical chemistry. *Atmos. Environ.* **124**, 207-216 (2016).

11. Huang, X. H. H., Ip, H. S. S., Yu, J. Z. Secondary organic aerosol formation from ethylene in the urban atmosphere of Hong Kong: A multiphase chemical modeling study. *J. Geophys. Res. Atmos.* **116**, D03206 (2011).

12. Sun, Y. et al. Rapid formation and evolution of an extreme haze episode in Northern China during winter 2015. *Sci. Rep.* **6**, 27151 (2016).

13. Herrmann, H. Kinetics of aqueous phase reactions relevant for atmospheric chemistry. *Chem. Rev.* **103**, 4691-4716 (2003).

14. Toda, K. et al. Formaldehyde content of atmospheric aerosol. *Environ. Sci. Technol.* **48**, 6636-6643 (2014).

15. Smith, A., Lott, N., Vose, R. The integrated surface database: recent developments and partnerships. *Bull. Amer. Meteor. Soc.* **92**, 704-708 (2011).

16. Global Modeling and Assimilation Office (GMAO). MERRA-2 tavg3_3d_cld_Np: 3d,3-Hourly,Time-Averaged,Pressure-Level,Assimilation,Cloud Diagnostics V5.12.4, Greenbelt, MD, USA, Goddard Earth Sciences Data and Information Services Center (GES DISC), Accessed [05/16/2018]. (2015).

17. Luan, T., Guo, X., Guo, L., Zhang, T. Quantifying the relationship between $PM_{2.5}$ concentration, visibility and planetary boundary layer height for long-lasting haze and fog–haze mixed events in Beijing. *Atmos. Chem. Phys.* **18**, 203-225 (2018).

18. Tie, X. et al. Severe pollution in China amplified by atmospheric moisture. *Sci. Rep.* **7**, 15760 (2017).

19. Zhong, J. et al. Feedback effects of boundary-layer meteorological factors on cumulative explosive growth of $PM_{2.5}$ during winter heavy pollution episodes in Beijing from 2013 to 2016. *Atmos. Chem. Phys.* **18**, 247-258 (2018).

20. Gross, D. S., Gälli, M. E., Silva, P. J., Prather, K. A. Relative sensitivity factors for alkali metal and ammonium cations in single-particle aerosol time-of-flight mass spectra. *Anal. Chem.* **72**, 416-422 (2000).

21. Ge, X., Zhang, Q., Sun, Y., Ruehl, C. R., Setyan, A. Effect of aqueous-phase processing on aerosol chemistry and size distributions in Fresno, California, during wintertime. *Environ. Chem.* **9**, 221-235 (2012).

22. Gilardoni, S. et al. Direct observation of aqueous secondary organic aerosol from biomass-burning emissions. *Proc. Natl. Acad. Sci. U.S.A.* **113**, 10013-10018 (2016).

23. Sander, R. Compilation of Henry's law constants (version 4.0) for water as solvent. *Atmos. Chem. Phys.* **15**, 4399-4981 (2015).

24. Olson, T. M., Hoffmann, M. R. Kinetics, mechanism and thermodynamics of glyoxal-sulfur(IV) adduct formation. *J. Phys. Chem.* **92**, 533-540 (1988).

25. Ip, H. S. S., Huang, X. H. H., Yu, J. Z. Effective Henry's law constants of glyoxal, glyoxylic acid, and glycolic acid. *Geophys. Res. Lett.* **36**, L01802 (2009).

26. Olson, T. M., Hoffmann, M. R. Formation kinetics, mechanism, and thermodynamics of glyoxylic acid-sulfur(IV) adducts. *J. Phys. Chem.* **92**, 4246-4253 (1988).

27. Betterton, E. A., Hoffmann, M. R. Henry's law constants of some environmentally important aldehydes. *Environ. Sci. Technol.* **22**, 1415-1418 (1988).

28. Winkelman, J. G. M., Voorwinde, O. K., Ottens, M., Beenackers, A. A. C. M., Janssen, L. P. B. M. Kinetics and chemical equilibrium of the hydration of formaldehyde. *Chem. Eng. Sci.* **57**, 4067-4076 (2002).

29. Ervens, B., Volkamer, R. Glyoxal processing by aerosol multiphase chemistry: towards a kinetic modeling framework of secondary organic aerosol formation in aqueous particles. *Atmos. Chem. Phys.* **10**, 8219-8244 (2010).

30. Sander, S. P., J. Abbatt, J. R. Barker, J. B. Burkholder, R. R. Friedl, D. M. Golden, R. E. Huie, C. E. Kolb, M. J. Kurylo, G. K. Moortgat, V. L. Orkin, P. H. Wine,. Chemical kinetics and photochemical data for use in atmospheric studies, evaluation no. 17. JPL Publication 10-6, Jet Propulsion Laboratory, Pasadena, http://jpldataeval.jpl.nasa.gov (2011).

31. Boyce, S. D., Hoffmann, M. R. Kinetics and mechanism of the formation of hydroxymethanesulfonic acid at low pH. *J. Phys. Chem.* **88**, 4740-4746 (1984).

32. Betterton, E. A., Hoffmann, M. R. Kinetics, mechanism and thermodynamics of the reversible reaction of methylglyoxal (CH_3COCHO) with sulfur(IV). *J. Phys. Chem.* **91**, 3011-3020 (1987).

33. Olson, T. M., Torry, L. A., Hoffmann, M. R. Kinetics of the formation of hydroxyacetaldehyde-sulfur(IV) adducts at low pH. *Environ. Sci. Technol.* **22**, 1284-1289 (1988).

34.   Deister, U., Neeb, R., Helas, G., Warneck, P. Temperature dependence of the equilibrium $CH_2(OH)_2 + HSO_3^-$ = $CH_2(OH)SO_3^- + H_2O$ in aqueous solution. *J. Phys. Chem.* **90**, 3213-3217 (1986).

35.   Dong, S., Dasgupta, P. K. On the formaldehyde-bisulfite-hydroxymethanesulfonate equilibrium. *Atmos. Environ.* **20**, 1635-1637 (1986).

36.   Kok, G. L., Gitlin, S. N., Lazrus, A. L. Kinetics of the formation and decomposition of hydroxymethanesulfonate. *J. Geophys. Res. Atmos.* **91**, 2801-2804 (1986).